INTERNATIONAL JOURNAL OF REFRIGERATION 75 (2017) 190–203

Available online at www.sciencedirect.com

ScienceDirect

journal homepage: www.elsevier.com/locate/ijrefrig

Experimental investigations of R134a and R123 falling film evaporation on enhanced horizontal tubes

Chuang-Yao Zhao, Pu-Hang Jin, Wen-Tao Ji, Ya-Ling He, Wen-Quan Tao *

Key Laboratory of Thermo-Fluid Science and Engineering, MOE, School of Energy and Power Engineering, Xi'an Jiaotong University, Xi'an 710049, China

ARTICLE INFO

Article history:
Received 18 April 2016
Received in revised form 20 December 2016
Accepted 21 December 2016
Available online 23 December 2016

Keywords:
Falling film evaporation
Boiling heat transfer
Refrigerant
Enhanced tube
R134a
R123

ABSTRACT

Falling film evaporation is an efficient heat transfer mode in refrigeration and air conditioning industries. In this paper, the falling film evaporation performances of R134a and R123 outside four enhanced tubes and a smooth tube are tested. The results reveal that: with the decrease of film flow rate the falling film heat transfer coefficients of both R134a and R123 on the five tubes exhibit two general stages (a plateau stage and a sharp drop stage); for R134a the plateau is quite uniform while for R123 a mild decrease occurs with the decrease in film flow rate. The four enhanced tubes behave differently in heat transfer performances for R134a and R123. R134a provides around 2–3 times of heat transfer coefficients of R123 for all tubes.

Étude expérimentale de l'évaporation du film tombant de r134a et de r123 sur un tube horizontal amélioré

Mots clés : Évaporation du film tombant ; Transfert de chaleur en ébullition ; Frigorigène ; Tube amélioré ; R134a ; R123

1. Introduction

There are two ways for improving the performance of flooded evaporator. One way is to use the so-called dry-evaporator in which liquid refrigerant goes through tube inside and water sits at the outside space of the evaporator; the other way is to adopt falling film evaporator where falling film evaporates outside horizontal tubes and water goes through tubes. The falling film evaporation is a relatively new way of combined single phase and boiling heat transfer and exhibits many advantages, including smaller refrigerant charge and efficient heat transfer characteristics at lower superheat. Therefore it has now attracted substantial attentions in refrigeration, air

* *Corresponding author.* Key Laboratory of Thermo-Fluid Science and Engineering, MOE, School of Energy and Power Engineering, Xi'an Jiaotong University, Xi'an 710049, China. Fax: +86 29 82669106.
E-mail address: wqtao@mail.xjtu.edu.cn (W.-Q. Tao).
http://dx.doi.org/10.1016/j.ijrefrig.2016.12.013
0140-7007/

Nomenclature

A	area [m^2]
Bo	modified boiling number
c_p	specific heat capacity [$Jkg^{-1}K^{-1}$]
D	diameter of tube [mm]
g	gravity acceleration [ms^{-2}]
h	heat transfer coefficient [$Wm^{-2}K^{-1}$]
k	overall heat transfer coefficient [$Wm^{-2}K^{-1}$]
L	tested length of tube [m]
$\dot{m}$	mass flow rate [kgs^{-1}]
Nu	Nusselt number
Pr	Prandtl number
P	Pressure [Pa]
q	heat flux [Wm^{-2}]
R	thermal resistance [m^2KW^{-1}]
r	latent heat [Jkg^{-1}]
Re	film Reynolds number
T	temperature [°C]
We	modified Weber number

Greek

Δ	variable differential
Γ	liquid film flow rate on one side of the tube per unit length [$kgm^{-1}s^{-1}$]
ϕ	heat transfer rate [W]
λ	thermal conductivity [$Wm^{-1}K^{-1}$]
μ	dynamic viscosity [$kgm^{-1}s^{-1}$]
ρ	density [kgm^{-3}]

Subscript

c	condensing
e	evaporating
l	liquid refrigerant
LMTD	logarithmic mean temperature difference
i	inside of tube
o	outside of tube
sat	saturation
w	wall

conditioning and petrochemical industries. In the process of falling film evaporation, the refrigerant is sprayed on the tube outside and evaporates, and then heat is transferred from tube side to shell side. Usually tube side fluid is water and its heat transfer coefficient is quite high. Thus, the level of heat transfer coefficient on the shell side is essential for the global performance of a falling film evaporator. In this paper some experimental results of falling film evaporation of two refrigerants outside some enhanced tube surface structures will be presented.

In the recent two decades evaporation and boiling heat transfer in liquid films falling on the heated tubes are increasingly investigated (Abed et al., 2015; Fernández-Seara and Pardiñas, 2014; Ribatski and Jacobi, 2005; Thome, 1999). In the early stage the studies were mainly concentrated on smooth tube and tube bundles. With the successful application of enhanced tube in pool boiling its application in the falling film evaporation has attracted more and more researchers' attentions. As indicated by Thome (1999), an optimal structure for enhancing falling film heat transfer applicable to a particular refrigerant is a challenge for the designers. In recent years, an increasing number of studies have focused on the falling film heat transfer performances on the enhanced tubes. The following section will present a brief summary on the progress of the falling film heat transfer with boiling on a single horizontal enhanced tube mainly in the chronological way.

To the authors' knowledge, the first application of enhanced tube to falling film evaporation is conducted by Fletcher et al. (1975), who obtained the higher heat transfer coefficient on knurled tube than smooth tube using distilled water. Han and Fletcher (1985) compared the heat transfer coefficients on the tubes with axial and circumferential grooves, and found that the circumferentially grooved tube provides better heat transfer performance. However, Sabin and Poppdndiek (1978) did not observe any enhanced effect of shallow axial grooves.

The above mentioned tubes were machined with 2-dimensional structures. Tubes with 3-dimensional structures were also studied by many researchers. Chyu and Bergles (1989) investigated the behaviors of Gewa-T, Thermoexcel-E and High Flux surfaces in both pool boiling and falling-film evaporation with water. Their results showed that generally speaking at the same wall superheat Gewa-T tube provides the highest heat flux, High Flux tube gives the lowest heat flux, while the heat flux of Thermoexcel-E tube is in between. Kuwahara et al. (1990) suggested that the Gewa-T tube is suitable for water boiling and the porous tube is a better choice for refrigerant boiling. According to the results of Tan et al. (1990), the JK2 tube provides 54%–190% higher heat transfer coefficient than that of the the JKl tube. Moeykens et al. (1995) reported that the condensation tubes (W-SC and Turbo-CII) have higher heat transfer coefficients than the boiling tubes (Turbo-B and W-SE). Liu and Yi (2001) compared the performance between 2-dimensional (low finned) and 3-dimensional structures (conical cavities), and found that the surfaces with 3-dimensional structures present a better performance at higher heat flux. The heat transfer coefficients as functions of heat flux available in studies of Fagerholm et al. (1987), Parken et al. (1990), Moeykens (1994) and Kim et al. (1998) are compared in Fig. 1.

Ribatski and Jacobi (2005) reviewed the measured results of enhanced tubes applied in falling film evaporation outside a single tube and tube bundle from 1976 to 2001, involving many commercial tubes originally designed for flooded evaporation (Turbo-B, Turbo-BII, High Flux and Thermoexcel-E), film condensation (Turbo-CII, Gewa-SE, Gewa-SC, Turbo-Chil and Thermoexcel-C) and low finned tubes. They found that the performance of an enhanced geometry is related to the work conditions and tube layout because of the different enhancement mechanisms under specified conditions.

Habert and Thome (2010) tested Gewa-B4 and found that the heat transfer performance has smaller dependence on heat flux. Christians and Thome (2012a) found that with increase of heat flux the heat transfer coefficient on Turbo-B5 increases while on Gewa-B5 obviously decreases. The effect of saturation temperature was not found in papers of Christians and Thome (2012a) and Habert and Thome (2010). Under the same work conditions, Moeykens (1994) evaluated the falling film evaporation performance of R134a, R22, and R123 on eight

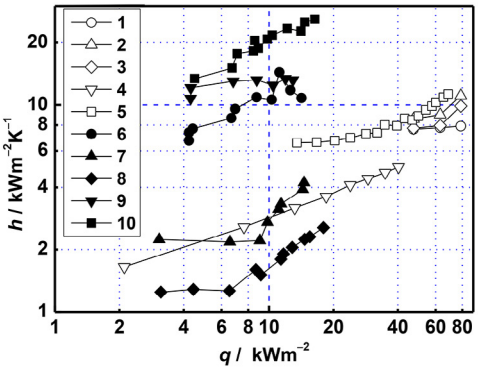

1-3: distilled water, 50–125 °C, smooth tube in Parken et al. (1990); 4: R134a, smooth tube, 2 °C in Moeykens (1994); 5: water, 120 °C in Kim et al. (1998); 6-10: R114, High Flux (6), sand-blasted (7), smooth (8), Gewa-T (9), Thermalexcel-E (10) in Fagerholm et al. (1987)

Fig. 1 – Falling film heat transfer coefficient versus heat flux with boiling.

commercial tubes. The results indicated that R134a provides around double heat transfer coefficient of R123, and that R22 behaves better than R134a on two surfaces. Chien and Tsai (2011) obtained slightly higher falling film heat transfer coefficient with R245fa than the one obtained in Moeykens et al. (1996) with R123 on a smooth tube. Chien and Tsai (2011) also compared the falling film heat transfer performances of R134 and R245fa on enhanced tubes with subcooling of 0.1–1.6 °C, and their results showed that R134a provides higher heat transfer coefficients than R245fa on the tube with smooth, mesh and 60 fpi finned surfaces. Christians and Thome (2012b) found that R134a provides better heat transfer performance than R236fa on Turbo-B5 and Gewa-B5 tubes.

Recently, Fernández-Seara and Pardiñas (2014) noted that most enhanced tubes not only improve falling film performance but also delay film breakdown compared with the smooth tube. According to the latest review conducted by Abed et al. (2015), there is few enhanced surfaces applicable to various applications of falling film evaporation because there is no universal principle that can be referenced for various work conditions.

The major influencing factors on the heat transfer coefficients of falling film evaporation on enhanced tube are the same as for the smooth tube, and they are: film flow rate, heat flux, tube diameter, saturation temperature and liquid distributor height on the enhanced tube (see Zhao et al., 2016a). Besides, the enhanced structures of the outer surface strongly influence the convective heat transfer and film distribution (Ribatski and Jacobi, 2005). The influences revealed by different authors can be summarized as follows: the heat transfer coefficient decreases with film flow rate at a lower heat flux due to increase in film thickness, while increases with film flow rate at a higher heat flux resulted from decrease in the dryout area (Zeng et al., 2000); before the occurrence of a film dryout a higher heat flux promotes heat transfer because of increased nucleation site density (Christians and Thome, 2012a; Fagerholm et al., 1987). The liquid distributor height has little influence on Thermoexcel-E, High Flux and Gewa-T tubes (Chyu and Bergles, 1985, 1989) at a high heat flux. While Zeng et al. (2001) obtained increased heat transfer coefficient with a larger nozzle height for a smooth tube.

According to the above review, several points can be confirmed: (1) The surface structures play predominant role in falling film heat transfer enhancement; (2) A specified enhanced structure has different enhancements under various operation conditions; (3) The low finned tube is not suitable for falling film evaporation since poor film distribution. In order to identify which type is suitable for falling film evaporation with specified conditions further experimental investigations on different enhanced tubes for different working refrigerants are highly needed.

In this paper, emphasis is placed on the falling film heat transfer characteristics of four horizontal enhanced tubes with different surface structures through experiments. The experiments are conducted using R134a and R123 under saturation temperature of 6 °C, film flow rate of 0.01 to 0.017 $kgm^{-1}s^{-1}$, and heat flux of 10 to 160 kWm^{-2}. Even though R123 may be phased out in near future, some common characteristics can be obtained from this study, such as the effects of viscosity and surface tension on falling film nucleate boiling and the applicability of the tube surface for different refrigerants.

The following sections will start with a brief description on the experimental system and test section. The experimental procedure will then be stated, followed by the data reduction and uncertainties analysis. After that the experimental results and discussion will be described. Finally some conclusions will be drawn.

2. Experimental facility and test tubes

2.1. *Test system*

The test rig is similar to the one used by Ji et al. (2016) and Zhao et al. (2016b), but in this study the boiler is closed. As schematically shown in Fig. 2, the experimental setup includes three circulation loops for refrigerant, heating water and cooling water, respectively.

2.2. *Refrigerant circuit*

During tests, the liquid refrigerant in liquid tank is pumped into the distributor and then is sprayed onto the test tube. The

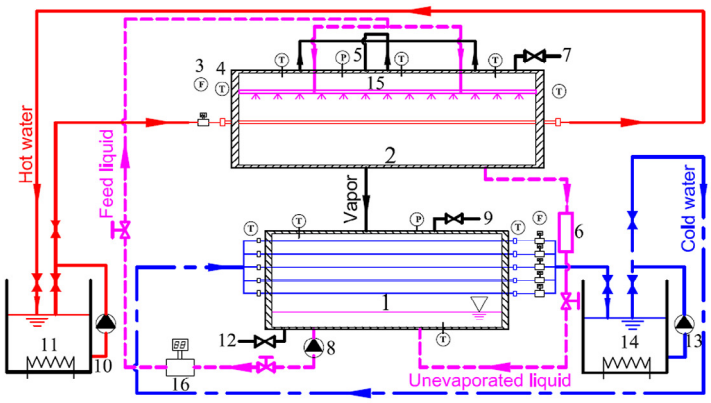

(1) Condenser & Liquid tank; (2) Evaporator; (3) Electromagnetic flowmeter; (4) RTDs; (5) Pressure gauge; (6) Condensate measuring container; (7) Exhausting valve; (8) Magnetic Pump; (9) Refrigerant charging valve; (10) Hot water pump; (11) Hot water tank; (12) Refrigerant outlet; (13) Cold water pump; (14) Cold water tank; (15) Liquid distributor.

Fig. 2 – Schematic diagram of the experimental system.

flow rate of the refrigerant pump can be adjusted by a frequency converter. Thereafter, the vapor flows into the condenser and the overfed liquid is also led into the condenser. The evaporator is a round vessel with an inner/outer diameter of 450/466 mm and a total length of 1450 mm, respectively. The condenser is a similar vessel having the same diameter as evaporator and a total length of 1140 mm. For insulation, the whole apparatus is carefully covered by rubber plastic material with 40 mm thick and then enwrapped with an aluminum foil layer.

2.3. *Water circuit*

The heating water temperature can be adjusted to a required value by heating and cooling unit in the water tank. Similarly, the cooling water circuit can provide cold water of required temperature with its own cooling and heating system. During running, the velocities of the heating and cooling water are controlled by their own bypass and a frequency converter.

2.4. *Instrumentation*

The flow rate of the liquid is measured by a Coriolis mass flow meter (SIEMENS MASS2100) with an accuracy of 0.1% of full scale. The flow rate of the heating water is measured by an electromagnetic mass flow meter (SIEMENS MAGFLO MAG5100W) with an accuracy of 0.1% of full scale.

During operations, the pressure of the system is measured by two pressure gauges (KELLER LEX1) with a measurement range of –0.1 ~ 2.0 MPa and an accuracy of 0.05% of the full scale fixed at the top and bottom of the evaporator. The temperatures of the vapor and liquid are measured by platinum resistance temperature transducers (Pt100) with an accuracy of ±(0.15 + 0.002|T|) K within the measurement range (*T* is the tested temperature). The temperatures of the water at tube's inlet and outlet are measured by ultra-precise RTD (OMEGA Pt100 1/10 DIN) with an accuracy of ± (0.03 + 0.0005|T|) K (*T* is the tested temperature) within the temperature range of this study. For data acquisition, a Keithley digital voltmeter of 0.1 μV resolution is used to measure the electric resistance.

2.5. *Liquid distributor*

The liquid distributor consists of two parts: the preliminary and secondary distributors. The liquid firstly flows into the preliminary distributor, flows out from its bottom orifices, and then flows into the secondary distributor and establishes a liquid level, finally sprays on the test tube after flowing out from its bottom orifices. The preliminary distributor is a rectangular stainless steel box. The secondary liquid distributor is another rectangular stainless steel box but with an upward opening. For the two boxes, many orifices with diameter of 2.0 mm and spacing of 20.0 mm are drilled at their bottom faces. The orifices diameter and spacing are designed carefully through preliminary tests to reach a uniform distribution performance by using water. When running, the pressure head provides falling momentum for the refrigerant liquid.

The details of the test system can be consulted in Ji et al. (2016) and Zhao et al. (2016a).

2.6. *Test tubes*

Four enhanced tubes are tested on this facility, including three enhanced boiling tubes with 3-D fins labeled as Nos. 1 to 3 and one enhanced condensing tube with 3-D fins labeled as No. 4. For the comparison and validation purpose one smooth tube is also tested. Five test tubes are made of copper and their specifications are listed in Table 1. As indicated, tube No.2 has the smallest fin density of 45 fpi (fins per inch) and tube No.4 has the largest fin density. Herein, the outlet widths of the reentrant cavity are also provided, which may influence the vapor departure. The fin types and scanning images of the four enhanced tubes are shown in Fig. 3. These tubes have a nominal external diameter of 19.0 mm, and an internal diameter of around 17.0 mm.

Table 1 – Specifications of five test tubes.

Tube	Outside diameter D_o (mm)	Inside diameter D_i (mm)	Height of outside fin e (mm)	Outside fins per inch	Outlet width of the reentrant cavity (mm)	Height of inside fin t (mm)	Length of test section (mm)
Smooth tube	19.06	17.19	—	—	—	—	535
No. 1	19.04	16.99	0.50	50	0.063	0.30	534
No. 2	18.89	16.61	0.57	45	0.119	0.32	500
No. 3	19.05	17.17	0.56	48	0.074	0.46	495
No. 4	19.03	17.00	0.71	51	0.280	0.34	535

3. Experimental procedure

After the test tube has been installed in the evaporator, high-pressure nitrogen is charged into the system until the internal pressure reaches double times of the working pressure, and then the pressure is maintained for 72 hours. If the pressure change of the system is less than 1 kPa, the system is evacuated to eliminate all non-condensable gases till the pressure is no more than 800 Pa (absolute). Finally, the refrigerant is charged in the system. During this operation, a small quantity of refrigerant is firstly charged and then evacuated again until the system pressure is less than 800 Pa. This operation should be repeated three times to make the quantity of the non-condensable gases as little as possible. After all the above preparations are completed, the refrigerant is charged to a required amount.

The tests are performed under saturation condition, which is realized by controlling the saturation temperature/pressure in the system. During operations, the liquid temperature in the tank of the distributor and the pressure in the system are measured. If the difference between the measured liquid temperature and the one correspondent to the measured pressure at the saturation line is less than 0.02 K, the saturation condition is regarded being reached and this measured liquid temperature is taken as the real saturation temperature. Experiments are conducted by gradually decreasing the liquid film flow rate on the tube at a fixed heat flux.

4. Data reduction and uncertainties analysis

4.1. *Heat balance*

For the test system heat is input by the heating water and output by the cooling water, denoted by ϕ_e and ϕ_c, respectively, which are defined as:

$$\begin{cases} \phi_e = \dot{m}_e c_p (T_{e,in} - T_{e,out}) \\ \phi_c = \dot{m}_c c_p (T_{c,out} - T_{c,in}) \end{cases} \quad (1)$$

In Eq. (1), $T_{e,\,in}$ and $T_{e,\,out}$ denote the temperatures of inlet and outlet hot water (K), respectively; $T_{c,in}$ and $T_{c,out}$ denote the temperatures of inlet and outlet cold water (K) through the tubes in condenser, respectively; $\dot{m}_e$ and $\dot{m}_c$ represent the mass flow rates of individual heating and cooling tube in two water circulations ($kgm^{-1}s^{-1}$), and c_p is the specific heat capacity ($Jkg^{-1}K^{-1}$) of water based on the mean temperature of inlet and outlet

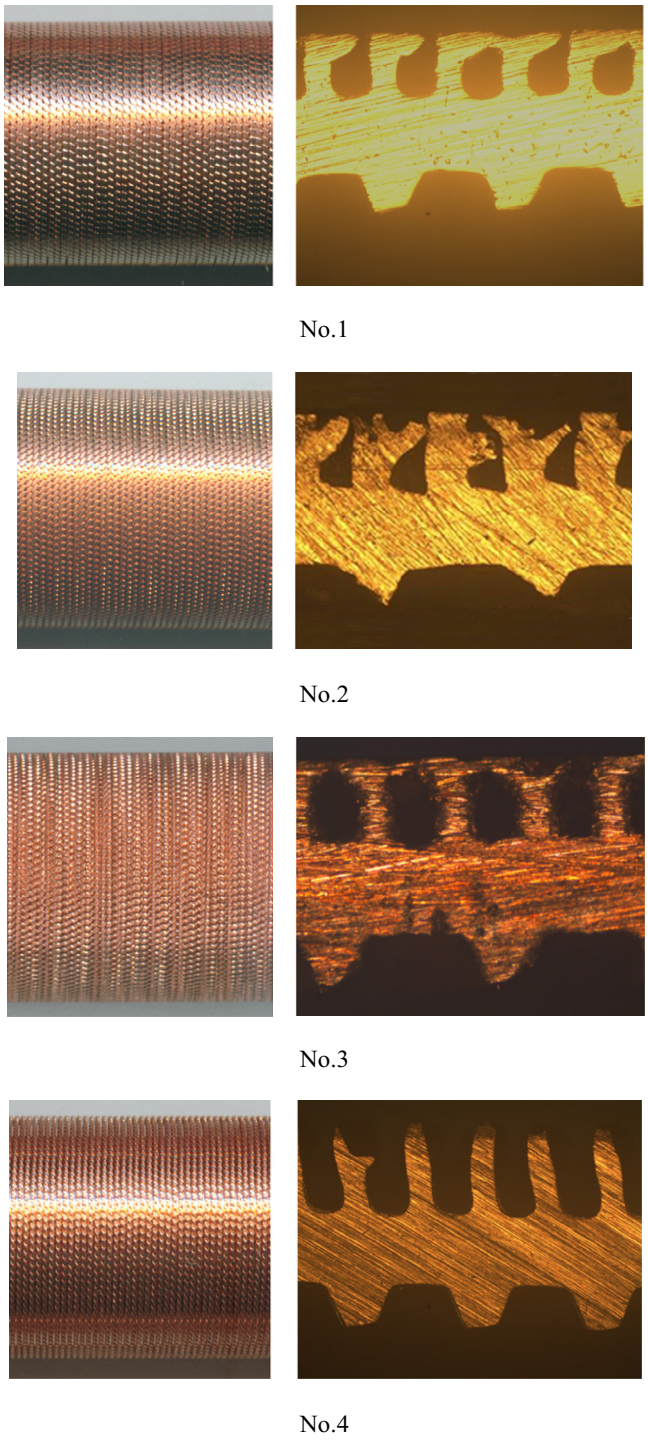

Fig. 3 – Geometries of enhanced tubes.

water. Considering the heat loss of the system to the surrounding, the heat balance in the system should meet the following equation:

$$(\phi_e + \phi_p - \phi_c)/\phi_a \le 5\% \quad (2)$$

where ϕ_p is the power of the magnetic gear pump which is immersed in the bulk of refrigerant liquid, 1.5 kW; ϕ_a is the reference heat transfer rate, defined by $\phi_a = (\phi_e + \phi_c + \phi_p)/2$.

4.2. *Heat transfer coefficient*

The overall heat transfer coefficient of the test tube is calculated by:

$$k = \frac{\phi_e}{A_o \Delta T_{LMTD}} \quad (3)$$

where ΔT_{LMTD} is the logarithmic mean temperature difference, defined as

$$\Delta T_{LMTD} = \frac{T_{e,in} - T_{e,out}}{\ln((T_{sat} - T_{e,out})/(T_{sat} - T_{e,in}))} \quad (4)$$

where T_{sat} is the saturation temperature. During utilization of this equation, the temperature difference of the hot water should be adequate to reduce test uncertainty. Taking the typical case with heat flux of 60 kWm^{-2} for example, the temperature difference is around 1.0 K.

According to the thermal resistance analysis method, Equation (3) can be written as:

$$\frac{1}{k} = \frac{1}{h_i}\frac{D_o}{D_i} + \frac{1}{h_o} + R_w \quad (5)$$

where D_i and D_o are the inner and outer diameters of the test tube, respectively; R_w is the thermal resistance of the wall; h_i is the inside convection heat transfer coefficient. Hence, the falling film heat transfer coefficient, h_o, can be expressed as

$$h_o = \left[\frac{1}{k} - \frac{1}{h_i}\frac{D_o}{D_i} - R_w\right]^{-1} \quad (6)$$

For the tube with enhanced inside structure, the inside convection heat transfer coefficient is calculated by:

$$h_i = c_i h_{gni} \quad (7)$$

In Eq. (7), c_i is enhanced factor of the internal surface, obtained by Wilson plot method, which is described in detail by Yang and Tao (2006). And h_{gni} is the inside heat transfer coefficient of the tube with smooth internal surface, which is determined by Gnielinski equation (Gnielinski, 1976; Yang and Tao, 2006) as:

$$h_{gni} = \frac{\lambda}{D_i}\frac{(f/8)(Re - 1000)Pr}{1 + 12.7(f/8)^{1/2}(Pr^{2/3} - 1)}\left[1 + \left(\frac{D_i}{L}\right)^{2/3}\right]\left(\frac{Pr}{Pr_w}\right)^{0.11} \quad (8)$$

(Re: 2300–10^6, Pr: 0.6–10^5).

In this paper, the film Reynolds number is determined by:

Table 2 – Experimental uncertainties of measured overall and falling film heat transfer coefficients.

Tube	q, kWm^{-2}	k, kWm^{-2}K^{-1}	h_o, kWm^{-2}K^{-1}
		δ_{max}	δ_{max}
Smooth	20	3.19%	15.4%
	40	3.18%	19.6%
	60	3.16%	24.0%
No. 1	20	3.23%	13.0%
	40	3.21%	13.6%
	60	3.19%	14.3%
No. 2	20	3.73%	14.2%
	40	3.22%	16.2%
	60	3.13%	15.4%
No. 3	20	3.24%	15.1%
	40	3.22%	15.1%
	60	3.09%	14.2%
No. 4	20	3.24%	19.3%
	40	3.21%	18.4%
	60	3.21%	20.2%

$$Re = \frac{4\Gamma}{\mu_l} \quad (9)$$

where Γ (kgm^{-1}s^{-1}) is the film flow rate on one side of the test tube per unit length.

4.3. *Uncertainty analysis*

The confidence analysis of the experimental data is carried out according to methods proposed by Cheng and Tao (1994) and Kline (1985). The uncertainty of overall heat transfer coefficient k for all data is less than 3.5% (see Table 2). The uncertainty of falling film heat transfer coefficients, h_o, is related to the ones of overall and inside heat transfer coefficient. Here the uncertainties of h_i is estimated by the Gnielinski equation whose uncertainty is within 10% (Cengel and Ghajar, 2011). For all experimental data, the percentage of water side thermal resistance varied from 28% to 55%. The thus-estimated uncertainty of h_o are shown in Table 2 for all the experimental data, with the maximum uncertainty being about 25%.

5. Results and discussion

5.1. *The inner side enhanced factor of the test tubes*

As shown in Eq. (7), the inner side enhanced factors for the four outside-enhanced tubes are obtained by using Wilson plot technique, in which the saturation temperature and heat flux are fixed and the inside water velocity is changed from 0.75 to 3.75 ms^{-1}. In this study, the heat flux $q = 50 \pm 0.5$ kWm^{-2} and saturation temperature $T_{sat} = 6 \pm 0.02$ °C. The same saturation temperature is adopted for both liquids for comparison purposes. After the test we can get a group of data about the overall thermal resistance and the inside thermal resistance for the smooth surface. For the four enhanced tubes, the two resistances, k^{-1} vs. h^{-1}, is plotted and their relationship can be well described by a straight line, as seen in Fig. 4. The slope of a line is equal to $D_o/(c_i D_i)$, from which the enhanced factor c_i can

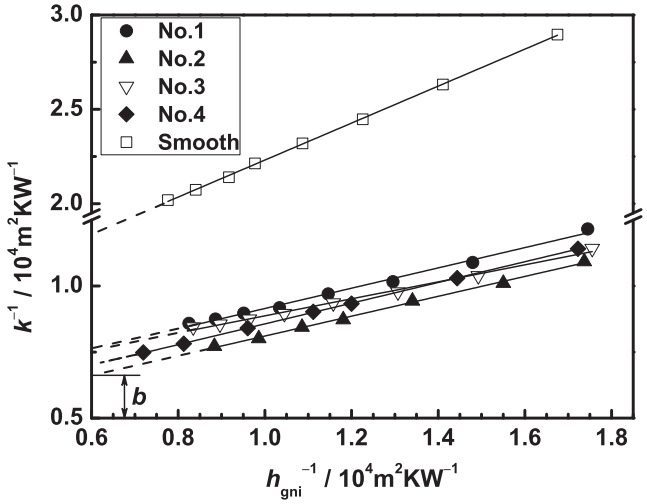

Fig. 4 – Wilson plots of the test tubes.

be obtained. And the intercept b is the sum of the thermal resistances of falling film evaporation and tube wall. The determined values of c_i are 2.90, 3.02, 3.45 and 2.84, respectively for the four internal enhanced tubes. In order to show the reliability of the method, the enhanced factor of the smooth tube is also got with the same method, as plotted in Fig. 4, whose c_i is 0.98, revealing good feasibility of the method. The different enhanced factors of the internal surfaces are related to the various parameters of the inside fins, such as the fin height, number of start, fin shape and helix angle.

5.2. *Falling film heat transfer coefficient*

5.2.1. *Smooth tube*

Fig. 5 shows the dependence of falling film heat transfer coefficients of the two refrigerants on the film flow rate for the smooth tube. The heat fluxes of the three curves are 20, 40 and 60 kWm^{-2}, respectively. From these curves, five features can be observed:

(1) For a fixed heat flux, the heat transfer coefficient gently descends with the decrease of film flow rate until reaches a turning point, and then rapidly drops with further decrease of film flow rate. The first descent stage can also be thought as a quasi-plateau one. The second dropping stage is caused by the increasing area of dryout. These findings are fully consistent with our previous test results for film cooling of R134a on a smooth tube (see Zhao et al., 2016a).

(2) At quasi-plateau stage, during increasing heat flux from 20 to 60 kWm^{-2} the heat transfer coefficient increases from an average of around 5.3 to 8.8 $kWm^{-2}K^{-1}$ for R134a and around 2.0 to 3.5 $kWm^{-2}K^{-1}$ for R123. The variation trend of the heat transfer coefficients with heat flux agrees with Zhao et al. (2016a).

(3) At the smaller film flow rate region (the drop stage), the heat transfer coefficients of the two refrigerants fall more rapidly at higher heat flux. This is because the film dryout becomes more severe at higher heat flux.

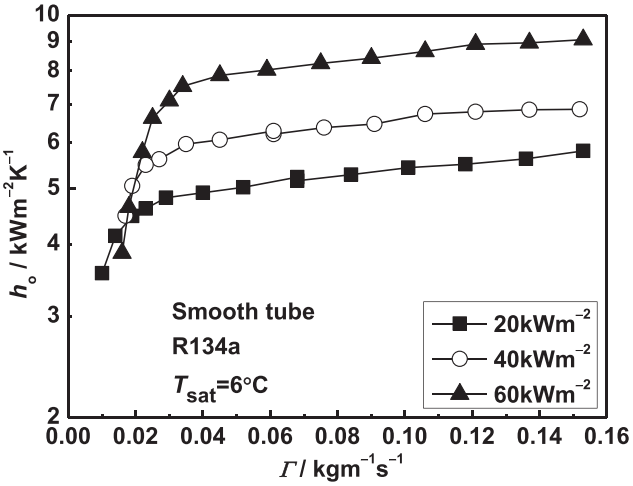

(a) R134a

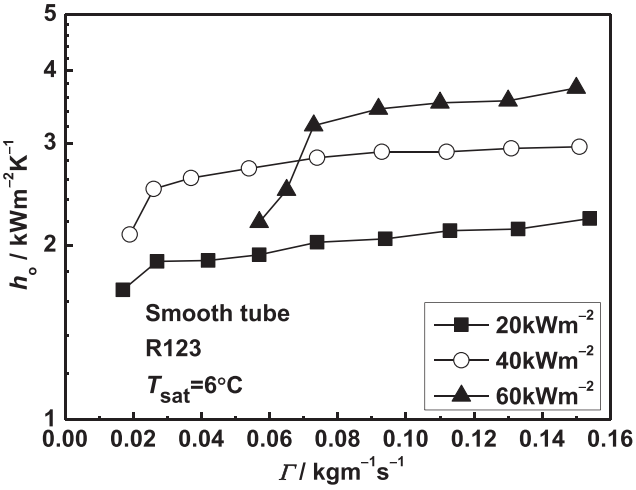

(b) R123

Fig. 5 – Falling film heat transfer coefficients of smooth tube versus film flow rate at different heat fluxes.

(4) There is a transition film flow rate at which the heat transfer coefficient trend varies from the first stage to the second one at each heat flux. With increase of heat flux from 20 to 60 kWm^{-2}, the transition film flow rate increases from around 0.025 to 0.035 kg $m^{-1}s^{-1}$ for R134a and around 0.025 to 0.07 kg $m^{-1}s^{-1}$ for R123. It is because at a larger heat flux more liquid is required to cover the tube wall, namely, a higher film flow rate. This phenomenon was also reported by Zhao et al. (2016a).

5.2.2. *Enhanced tubes*

For enhanced tubes Nos. 1 to 4, the variations of falling film heat transfer coefficients of the two refrigerants versus film flow rate at three heat fluxes are presented in Figs. 6–9. In these figures, the global variation trends of the heat transfer coefficients against the film flow rates are quite similar to that for the smooth tube. However, some other features can also be noted:

(1) In the larger film flow rate region, the heat transfer coefficients are almost independent of film flow rate. This different characteristic from the smooth tube seems to be related to the improved film distribution on the enhanced tube: the interconnected cavities on the enhanced tube are more favorable than the smooth tube to uniform film distribution, which makes the enhanced tube less sensitive to the reduction of film flow rate.
(2) For R134a, with increase of heat flux, the heat transfer coefficients of four tubes exhibit different trends. For tubes Nos. 1, 3 and 4, the increasing heat flux promotes falling film heat transfer monotonously. While for tube No. 2, with increase of heat flux the heat transfer coefficient is firstly enhanced and then decreased, as found in Ji et al. (2016) by using the same tube. These different dependences on heat flux should be related to the surface structure. As shown in Fig. 3, there are some branches (secondary fins) on the fins of tube No. 2, which may do harm to heat transfer at higher heat flux.
(3) For R134a, the transition film flow rate on the enhanced tube is slightly smaller than the ones on the smooth tube. For the four tubes all transition film flow rates at three fluxes are about 0.025 $kgm^{-1}s^{-1}$, while for smooth tube the transition film flow rates are within 0.025 to 0.035 $kgm^{-1}s^{-1}$. This difference implies that the enhanced surfaces can delay the film dryout at a given heat flux compared with the smooth surface, of which the reason is similar to item (1) in this section.
(4) For R123 in the current film flow rate range, quasi-plateau stages are seen for the heat transfer coefficients of the four enhanced tubes with the reduction of film flow rate, which is similar to the one of R134 on the smooth tube. In the test range of heat fluxes and film flow rates, the transition from the plateau to the sharp drop of the heat transfer coefficient occurs at a smaller film flow rate, around 0.02 to 0.025 $kgm^{-1}s^{-1}$.

5.3. *Performance comparisons for different enhanced tubes*

For the comparison among all tested enhanced tubes, the results at heat flux of 40 kWm^{-2} are plotted together in Fig. 10 for the two refrigerants, with the results of the smooth tube as a reference. We can find the following two points:

(1) For R134a, tubes Nos. 2 and 4 have the highest heat transfer coefficients, the heat transfer coefficient of tube No. 1 is the worst, while that of tube No. 3 is in between.
(2) For R123, the ranks of the heat transfer performances of the tubes are different from R134a, the best tubes are Nos. 1 and 3, the moderate tube is No. 2, and the worst tube is No. 4.

According to the specifications of the enhanced tubes shown in Table 1, it can be seen that tubes Nos. 2 and 4 with larger outlet width of the reentrant cavity are favorable for heat transfer of R134a while tubes Nos. 1 and 3 with smaller outlet width of the reentrant cavity are favorable for heat transfer of R123. The different rankings of the heat transfer coefficients of the two refrigerants probably attribute to different film distributions on the same surface, while the detailed reason needs further study.

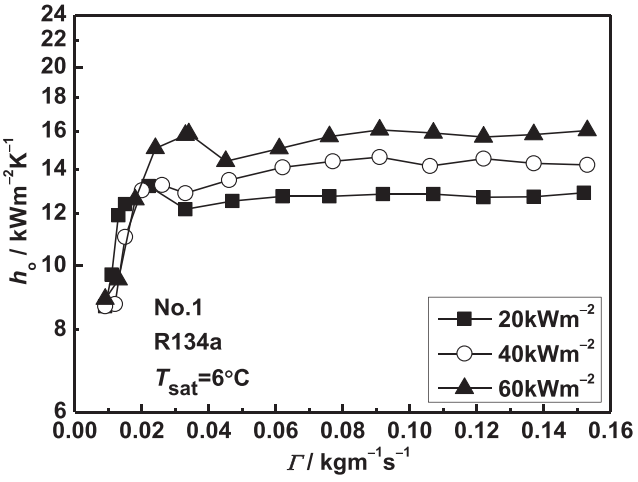

(a) R134a

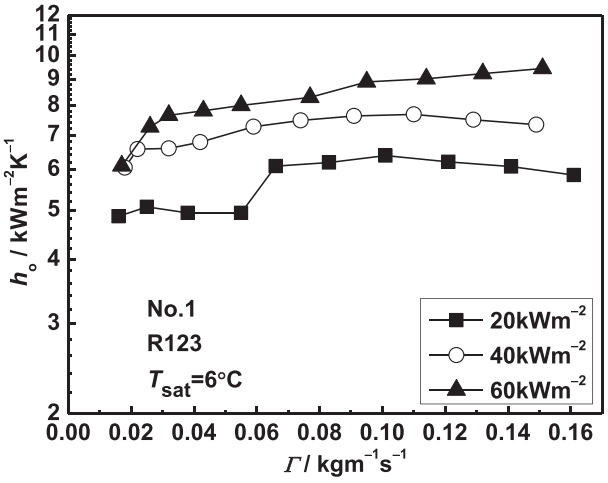

(b) R123

Fig. 6 – Falling film heat transfer coefficients of enhanced boiling tube No. 1 versus film flow rate at different heat fluxes.

It is interesting to note that in the presentation shown in Figs. 5–10, some differences between different test conditions are not very large and may be smaller than the maximum test uncertainty. However, all the data shown in these figures are consistent and in good variation trends. Hence these test data are irrefutable.

The results of the present study and the ones available in the literature are compared in Fig. 11 with the form of h_o versus q.

In Fig. 11 (a), the results of R134a obtained by Moeykens et al. (1995), Roques and Thome (2007a), Habert and Thome (2010) and Christians and Thome (2012a) are depicted. For these studies, the saturation temperature are 2.0–6.0 °C, the film Reynolds numbers are 200–580, and the involved tubes are Turbo-B, Turbo-CII, W-SE, W-SC, W-40 fpi, W-26 fpi, Turbo-BII HP, Gewa-B, High Flux, Gewa-B5, Turbo-B5, Gewa-CLW, Gewa-B4 and

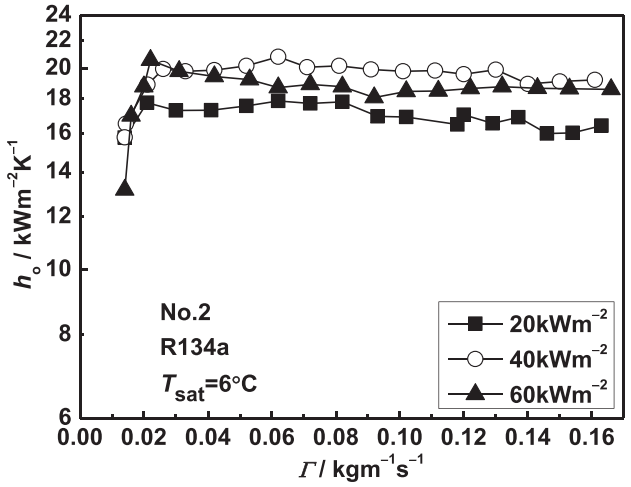

(a) R134a

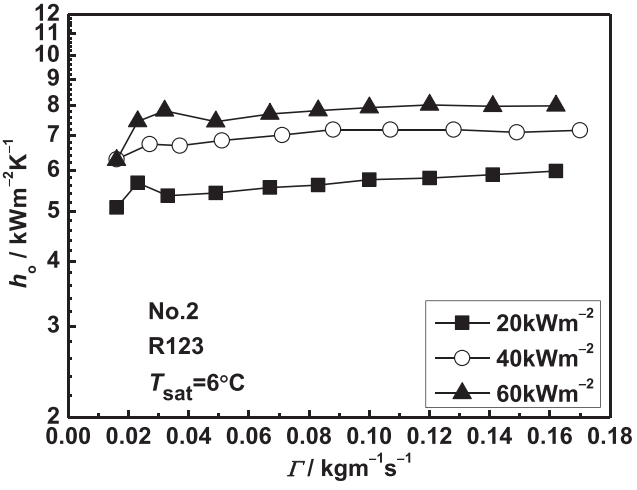

（b）R123

Fig. 7 – Falling film heat transfer coefficients of enhanced boiling tube No. 2 versus film flow rate at different heat fluxes.

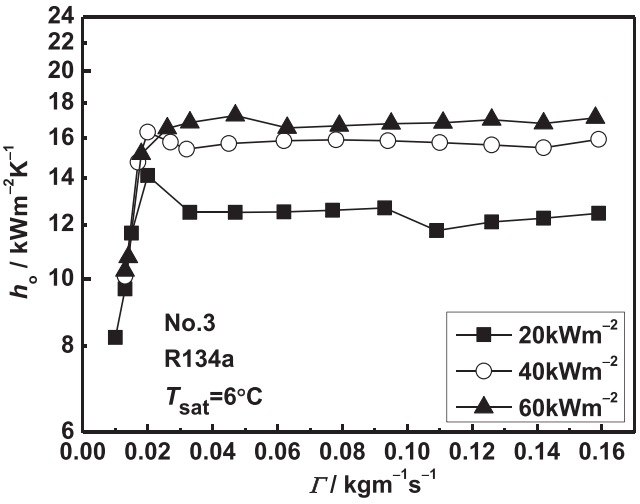

(a) R134a

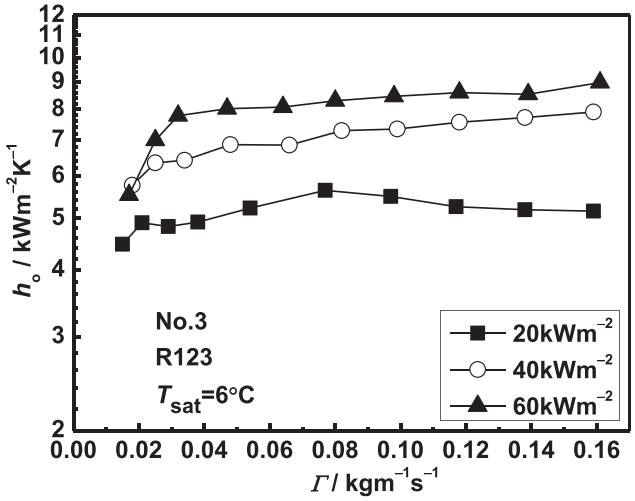

（b）R123

Fig. 8 – Falling film heat transfer coefficients of enhanced boiling No. 3 versus film flow rate at different heat fluxes.

Turbo-EDE2. From this figure, we can note that: (1) For the smooth tube and enhanced tubes of the present study, with increase of heat flux there are three stages for the heat transfer coefficients: rapidly increase, stable stages (with developed nucleate boiling) and slightly decline (with partial film dryout), between which there are two transition heat fluxes, and the two transition heat fluxes are dependent on the enhanced surface types; (2) For the tubes of Moeykens et al., the tubes of Turbo-CII and W-SC have higher heat transfer coefficients, and the lower finned tube with 26 fpi is better than the one with 40 fpi; (3) At lower heat flux range, the heat transfer coefficients of Moeykens et al. are less dependent on heat flux than other tubes; (4) For the tubes of Thome's group, with increase of heat flux the heat transfer coefficient of Gewa-CLW slightly increases while the ones of other tubes significantly decrease; (5) Compared with the smooth tube, the heat transfer enhanced ratios (ratio between the enhanced tube and the smooth) of the present four enhanced tubes, Moeykens et al. and Thome's group are 2–4, 1.5–2 and 3–10, respectively.

Similarly, the variations of falling film heat transfer coefficients of R123 with heat flux in the present study and the ones of Moeykens et al. (1996) are compared in Fig. 11 (b), where film Reynolds numbers are 248–392 and saturation temperatures are 2.0–6.0 °C. In the figure the pool boiling heat transfer coefficients on smooth tube in Webb and Pais (1992) are also presented. From this figure it can be seen that: (1) The heat transfer coefficient of the present smooth tube reaches the comparative level as that of Moeykens et al. (1996) and is higher than the pool boiling heat transfer coefficient; (2) In the current heat flux range all enhanced tubes provide higher heat transfer coefficients than the smooth tube; (3) For the four enhanced tubes in the present study, the heat transfer coefficients first increase and then decrease with the increase of heat flux, with the heat transfer coefficient of tube No. 1 being the smallest

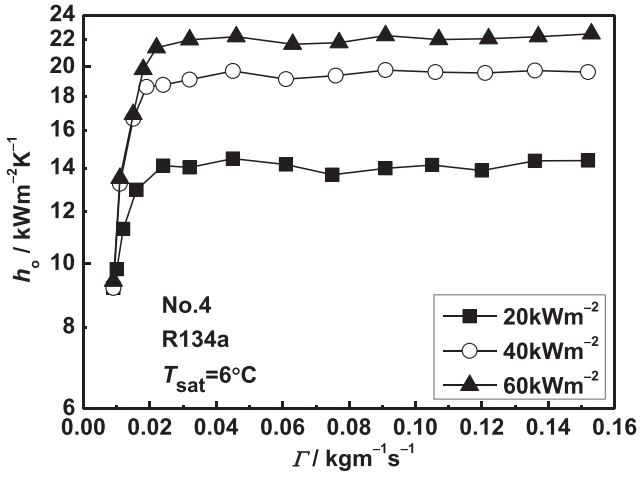

(a) R134a

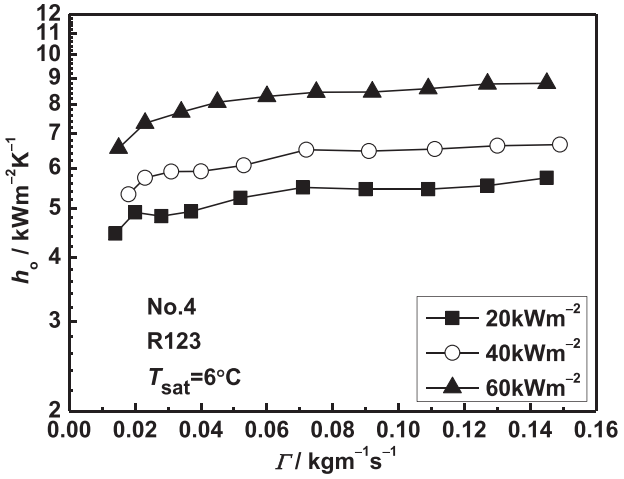

(b) R123

Fig. 9 – Falling film heat transfer coefficients of enhanced boiling No. 4 versus film flow rate at different heat fluxes.

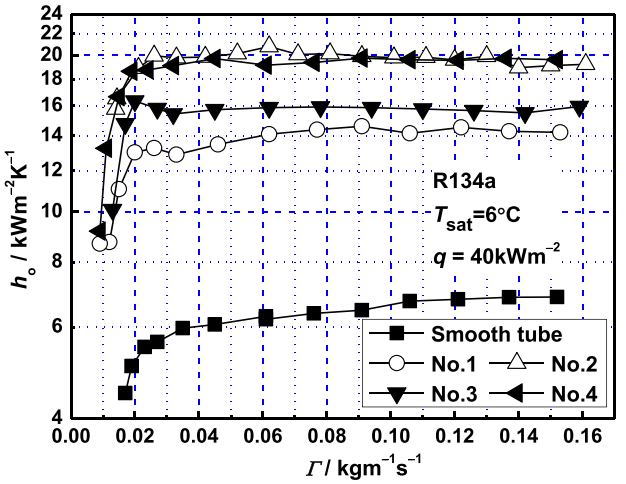

(a) R134a

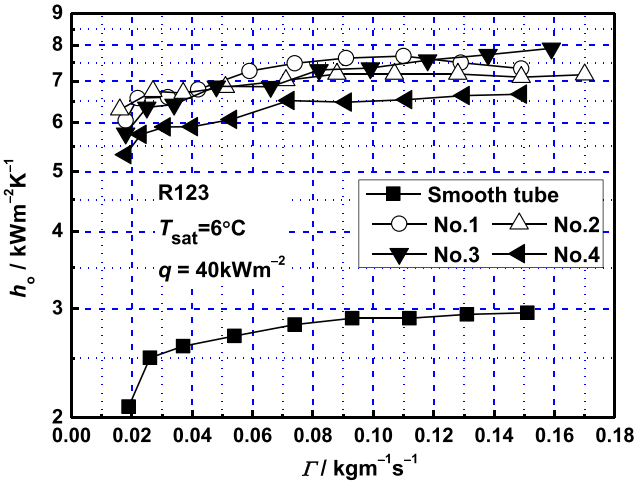

(b) R123

Fig. 10 – Comparison among of falling film heat transfer coefficients for five test tubes at heat flux of 40 kWm^{-2}.

when $q > 60$ kWm^{-2}. And in the heat flux range studied, the four tubes have significant enhancing function compared with smooth tube; (4) For the tubes of Moeykens et al. (1996), Turbo-B provides more than two times heat transfer coefficient of that of Turbo-CII; (5) The heat transfer coefficients of Turbo-B and Turbo-CII are much higher than that of the present four enhanced tubes, which may be caused by three reasons: film flow rates of Moeykens et al. (1996) are larger than those of the present study (Reynolds number of 392 vs. 248) the different tube surfaces of these tubes and the different film distributors.

The nucleate boiling on the enhanced tube is a major research field in refrigeration. The study of nucleate boiling heat transfer on the enhanced surfaces involves many complexities. And these complexities are probably related to some micromechanisms of bubble growth and molecular dynamics of nucleation. Actually, in order to better understand the effects of enhanced structures on the nucleate boiling our group have been making efforts to study the bubble's behavior in nucleate boiling using the coupled Volume-of-Fluid and Level Set (VOSET) method (Ling et al., 2014) and the boiling process in cavities by using Lattice Boltzmann method (LBM) (Mu et al., 2017). Furthermore for the falling film evaporation with nucleate boiling the heat transfer rate consists of single phase convective heat transfer and nucleate boiling, making the mechanism more complicated. Thus for the time being it is very difficult to explain the different performance of the different enhanced tubes tested in this study. The major purpose of the present study is to provide reliable test data, which will be very helpful for the comparison with numerical simulation results.

5.4. *Comparison between the two refrigerants*

Experimental results in Figs. 5–9 show that the heat transfer coefficients of R134a are about two times of R123 at the identical conditions especially for the cases with larger film flow rate. It is worth noting here that the uncertainty is relatively insignificant compared with the difference in heat transfer

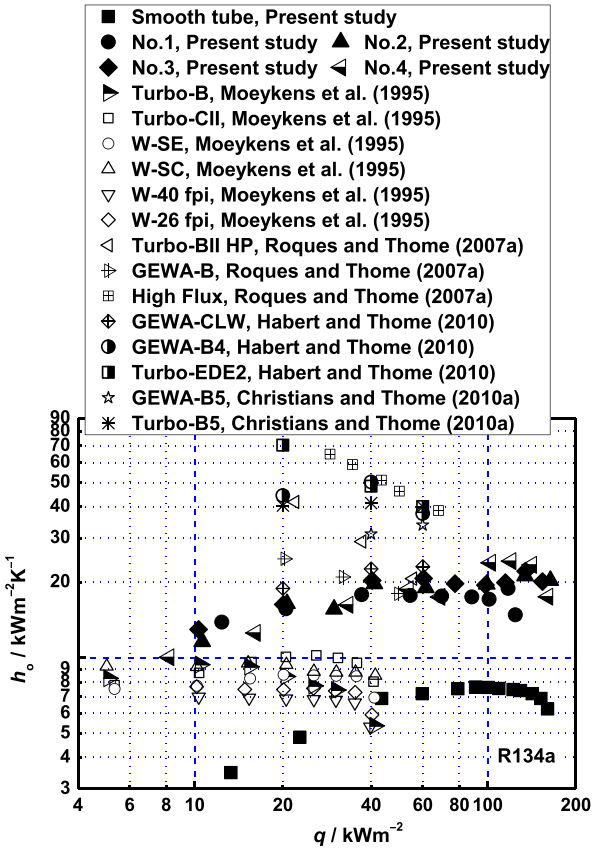

（a）R134a, present study: Re = 540, T_{sat} = 6 °C; Moeykens et al. (1995) Re = 200, T_{sat} = 2 °C; Thomes's group (2007 to 2010): Re = 580, T_{sat} = 5 °C

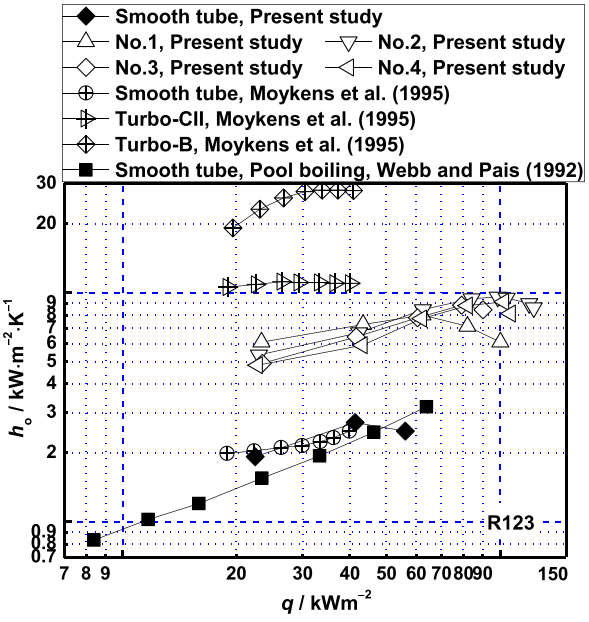

（b）R123, present study: Re = 248, T_{sat} = 6 °C; Moeykens et al. (1995) Re = 392, T_{sat} = 2 °C

Fig. 11 – Falling film heat transfer coefficients versus heat flux.

Table 3 – Threshold film Reynolds number for the cases of smooth tube.

Case	R134a			R123		
	20 kWm^{-2}	40 kWm^{-2}	60 kWm^{-2}	20 kWm^{-2}	40 kWm^{-2}	60 kWm^{-2}
$Re_{threshold\text{-}Pre}$	295	427	470	> Re_{max}	> Re_{max}	> Re_{max}

coefficients of the two refrigerants. The great gap can be explained by following considerations.

The vapor density of R134a is about six times of R123, which means that for generation of a bubble with the same volume R134a needs much larger energy than R123 at the identical conditions considering the similar latent heat of the two fluids.

In addition, following understanding further suggests that R134a should have a larger boiling heat transfer coefficient. For nucleate boiling occurring in the thin film on the heating wall, In and Jeong (2009) recommended using the wall superheat equation derived by Davis and Anderson (1966) to calculate the wall superheat requirement for nucleate boiling. The wall superheat ($T_w - T_{sat}$) corresponding to an imposed heat flux is expressed by:

$$T_w - T_{sat} = \frac{R \cdot T_{sat}^2 \cdot \ln(1+\xi)/(r \cdot M)}{1 - R \cdot T_{sat} \cdot \ln(1+\xi)/(r \cdot M)} + \frac{q \cdot r_a}{\lambda_l}, \quad \xi = \frac{2 \cdot \sigma}{P_{sat} \cdot r_a} \tag{10}$$

where, R is the universal gas constant, M is the molecular weight, r_a is the maximum active cavity size, r is the latent heat, σ is the surface tension and P_{sat} is the saturation pressure. According to In and Jeong (2009), the larger surface tension and smaller saturation pressure of R123 produce higher superheat requirement for R123 than R134a under the identical heat flux, which make the poorer nucleate boiling heat transfer in R123.

Finally, the convective heat transfer rate is proportional to –0.4 power of viscosity and 0.6 power of heat conductivity, which leads around 30% lower heat transfer coefficient of R123 than R134a, and this is also a reason for the great gap between the two refrigerants.

5.5. *Comparison with previous correlation*

The heat transfer coefficients of the present smooth tube are compared with the correlation proposed by Zhao et al. (2016a), in which the heat transfer coefficients are predicted by the following two equations:For the partial dryout case:

$$Nu = 4.64 \times 10^{-3} Re^{1.51} Bo^{0.43} Pr^{0.15} We^{-0.45} \tag{11}$$

and for the full wetted case:

$$Nu = 3.58 \times 10^{-9} Re^{2.89} Bo^{0.37} Pr^{0.2} We^{-1.13} \tag{12}$$

where, Nusselt number $Nu = h_o D_o/\lambda_l$, film Reynolds number $Re = 4\Gamma/\mu_l$, Prandtl number $Pr = \mu_l c_p/\lambda_l$, Boiling number $Bo = qD_o/r\Gamma$, and modified Weber number $We = \frac{\Gamma^2}{\pi^2(\rho_l - \rho_v)D_o\sigma}$.

The threshold film Reynolds number beyond which the flow is fully wetted is also proposed by Zhao et al. (2016a) as follows:

$$Re = 5.36 \times 10^4 Bo^{0.0045} Pr^{-0.52} We^{0.5} \tag{13}$$

The threshold film Reynolds number for individual data is firstly calculated by Eq. (13) according to the test conditions, and the results are listed in Table 3. From the test conditions provided the values of *Bo*, *Pr* and *We* can be determined and hence the values of threshold Reynolds number can be obtained with ease. In Table 3 Re_{max} denotes the largest *Re* of the data. And therefore the data of the smooth tube are classified into two categories: some data of R134 are classified as full wetted case, the rest of the data of R134 and all data of R123 are classified as partial dryout case. Fig. 12 shows the ratios of the present Nusselt numbers to the predicted ones by using

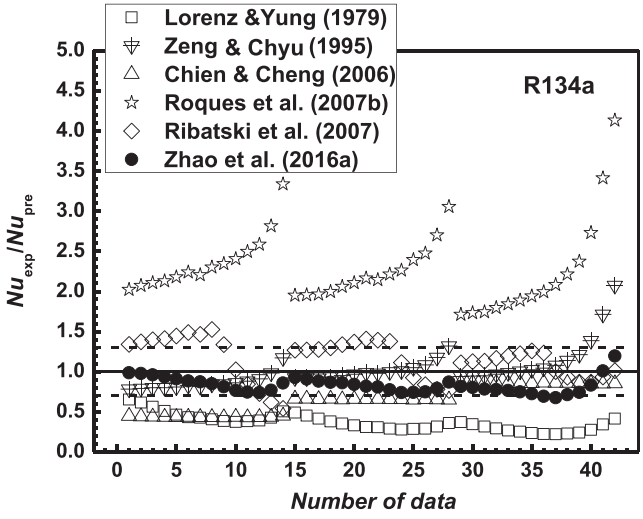

(a) R134a

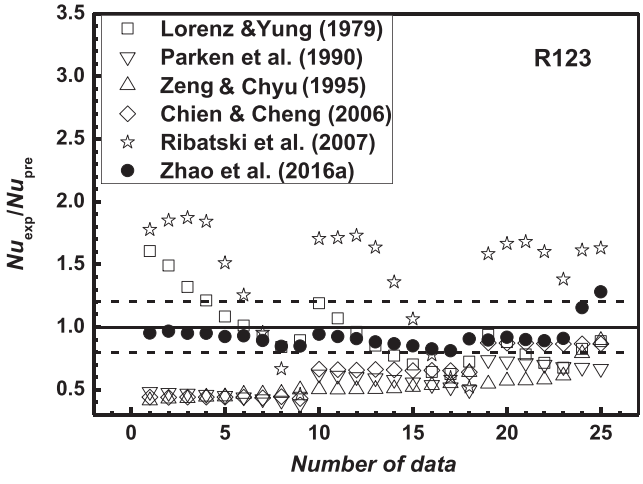

(b) R123

Fig. 12 – Comparison of the present results with previous correlations of smooth tube.

Eqs. (11) and (12) proposed by Zhao et al. (2016a) and other published correlations (Lorenz and Yung, 1979; Parken et al., 1990; Zeng and Chyu, 1995; Chien and Cheng, 2006; Ribatski and Thome, 2007; Roques and Thome, 2007b). It can be seen: (1) The correlations of Zhao et al. (2016a) predict almost all data (93% of 42 data) with deviation within 30% for R134a (Fig. 12(a)) and 20% for R123 (Fig. 12(b)); (2) For R134a, the correlations of Zeng and Chyu (1995), Chien and Cheng (2006) and Ribatski and Thome (2007) can predict most data with deviations within 50%, with some data much under- or overestimations; (3) For R123, the agreement situations are much worse and only the correlation by Zhao et al. (2016a) can keep most deviations within ±20%. It is worth pointing out that the correlations of Ribatski and Thome (2007) and Roques and Thome (2007b) are established based on tube array or bundle, and thus the overestimations are severe because of the bundle effects.

6. Conclusions

In this paper, the falling film evaporation of R134a and R123 outside four enhanced horizontal tubes and a smooth tube is experimentally investigated. Based on the results, the following conclusions can be drawn:

(1) For R134a on the enhanced tubes, with decrease of film flow rate the falling film heat transfer coefficients on the four tubes exhibit two general stages: at a larger film flow rate a plateau stage and at a smaller film flow rate a sharp drop stage.
(2) For R134a on the smooth tube and for R123 on all tubes, the variation of falling film heat transfer coefficients with the film flow rate shows a quasi-plateau stage and a rapid drop stage.
(3) At the same test condition, R134a provides around 2–3 times of heat transfer coefficients of those of R123 at the film flow rate region larger than 0.025 $kgm^{-1}s^{-1}$.
(4) At the larger film flow rate region, with increase of heat flux the falling film heat transfer of R134a is promoted monotonously on tubes Nos. 1, 3 and 4, while it is firstly promoted and then suppressed on the tube No. 2. However, the heat transfer coefficients of R123 increase with heat flux for all tubes.
(5) For R134a, tubes Nos. 2 and 4 provide higher heat transfer coefficients than tubes Nos. 1 and 3. For R123, tubes Nos. 1 and 3 provide a better falling film evaporation performance than tubes Nos. 2 and 4.
(6) The data of R134 and R123 on smooth tube can be relatively better predicted by the heat transfer correlation of Zhao et al. (2016a) than other five correlations available in the literatures.

Acknowledgments

This work was supported by the National Key Basic Research Program of China (973 Program) (2013CB228304) and the Research Fund for the Doctoral Program of Higher Education of China (20120201130007)

REFERENCES

Abed, A.M., Alghoul, M.A., Yazdi, M.H., Al-Shamani, A.N., Sopian, K., 2015. The role of enhancement techniques on heat and mass transfer characteristics of shell and tube spray evaporator: a detailed review. Appl. Therm. Eng. 75, 923–940.
Cengel, Y.A., Ghajar, A.J., 2011. Heat and Mass Transfer, Fundamentals and Applications, fourth ed. McGraw-Hill, New York.
Cheng, B., Tao, W.Q., 1994. Experimental study of R-152a film condensation on single horizontal smooth tube and enhanced tubes. ASME J. Heat Transfer 116, 266–270.
Chien, L.H., Cheng, C., 2006. A predictive model of falling film evaporation with bubble nucleation on horizontal tubes. HVAC&R Res 12, 69–87.
Chien, L.H., Tsai, Y.L., 2011. An experimental study of pool boiling and falling film vaporization on horizontal tubes in R-245fa. Appl. Therm. Eng. 31, 4044–4054.
Christians, M., Thome, J.R., 2012a. Falling film evaporation on enhanced tubes, part 1: experimental results for pool boiling, onset-of-dryout and falling film evaporation. Int. J. Refrigeration 35, 300–312.
Christians, M., Thome, J.R., 2012b. Falling film evaporation on enhanced tubes, part 2: prediction methods and visualization. Int. J. Refrigeration 35, 313–324.
Chyu, M.C., Bergles, A.E., 1985. Enhancement of horizontal tube spray film evaporators by structured surfaces. Adv. Enhanc. Heat Transfer 43, 39–47.
Chyu, M.C., Bergles, A.E., 1989. Horizontal-tube falling-film evaporation with structured surfaces. ASME J. Heat Transfer 111, 518–614.
Davis, E.J., Anderson, G.H., 1966. The incipience of nucleate boiling in forced convection flow. AIChE J. 12, 774–780.
Fagerholm, N.E., Ghazanfari, A.R., Kivioja, K., Järvinen, E., 1987. Boiling heat transfer performance of plain and porous tubes in falling film flow of refrigerant R114. Heat Mass Transf. 21, 343–353.
Fernández-Seara, J., Pardiñas, Á.Á., 2014. Refrigerant falling film evaporation review: description, fluid dynamics and heat transfer. Appl. Therm. Eng. 64, 155–171.
Fletcher, L.S., Sernas, V., Parken, W.H., 1975. Evaporation heat transfer coefficients for thin sea water films on horizontal tubes. Ind. Eng. Chem. Proc. Des. Dev. 14, 411–416.
Gnielinski, V., 1976. New equations for heat and mass transfer in the turbulent flow in pipes and channels. Int. Chem. Eng. 16, 359–368.
Habert, M., Thome, J.R., 2010. Falling-film evaporation on tube bundle with plain and enhanced tubes: part I: experimental results. Exp. Heat Transfer 23, 259–280.
Han, J.C., Fletcher, L.S., 1985. Falling film evaporation and boiling in circumferential and axial grooves on horizontal tubes. Ind. Eng. Chem. Proc. Des. Dev. 24, 570–575.
In, S., Jeong, S., 2009. Flow boiling heat transfer characteristics of R123 and R134a in a micro-channel. Int J Multiph. Flow. 35, 987–1000.
Ji, W.T., Zhao, C.Y., Zhang, D.C., Yoshioka, S., He, Y.L., Tao, W.Q., 2016. Effect of vapor flow on the falling film evaporation of R134a outside a horizontal tube bundle. Int. J. Heat Mass Transf. 92, 1171–1181.
Kim, J.O., Kim, N.H., Choi, K.K., 1998. Thin film evaporation on horizontal plain tubes. Sol. Energy 18, 49–57.
Kline, S.J., 1985. The purposes of uncertainty analysis. ASME J. Fluid. Eng. 107, 153–160.
Kuwahara, H., Yasukawa, A., Nakayama, W., Yanagida, T., 1990. Evaporative heat transfer from horizontal enhanced tubes in thin film flow. Heat Transfer Jpn. Res. 19, 83–97.

Ling, K., Li, Z.Y., Tao, W.Q., 2014. A direct numerical simulation for nucleate boiling by the VOSET method. Numer. Heat Transfer Part A. 65, 949–971.
Liu, Z.H., Yi, J., 2001. Enhanced evaporation heat transfer of water and R-11 falling film with the roll-worked enhanced tube bundle. Exp. Therm. Fluid Sci. 25, 447–455.
Lorenz, J.J., Yung, D., 1979. A note on combined boiling and evaporation of liquid films on horizontal tubes. ASME J. Heat Transfer 101, 178–180.
Moeykens, S.A., 1994. Heat transfer and fluid flow in spray evaporators with application to reducing refrigerant inventory. Iowa State University. Iowa State University.
Moeykens, S.A., Huebsch, W.W., Pate, M.B., 1995. Heat transfer of R-134a in single-tube spray evaporation including lubricant effects and enhanced surface results. ASHRAE Trans. 101, 111–123.
Moeykens, S.A., Kelly, J.E., Pate, M.B., 1996. Spray evaporation heat transfer performance of R-123 in tube bundles. ASHRAE Trans. 102, 259–272.
Mu, Y.T., Chen, L., He, Y.L., Kang, Q.J., Tao, W.Q., 2017. Nucleate boiling performance evaluation of cavities at mesoscale level. Int. J. Heat Mass Transf. 106, 708–719.
Parken, W.H., Fletcher, L.S., Han, J.C., Sernas, V., 1990. Heat transfer through falling film evaporation and boiling on horizontal tubes. ASME J. Heat Transfer 112, 744–750.
Ribatski, G., Jacobi, A.M., 2005. Falling-film evaporation on horizontal tubes – a critical review. Int. J. Refrigeration 28, 635–653.
Ribatski, G., Thome, J.R., 2007. Experimental study on the onset of local dryout in an evaporating falling film on horizontal plain tubes. Exp. Therm. Fluid Sci. 31, 483–493.
Roques, J.F., Thome, J.R., 2007a. Falling films on arrays of horizontal tubes with R-134a, part I: boiling heat transfer results for four types of tubes. Heat Transfer Eng. 28, 398–414.
Roques, J.F., Thome, J.R., 2007b. Falling films on arrays of horizontal tubes with R-134a, part II: flow visualization, onset of dryout, and heat transfer predictions. Heat Transfer Eng. 28, 415–434.
Sabin, C.M., Poppdndiek, H.F., 1978. Film evaporation of ammonia over horizontal round tubes, Proceedings of the 5th Ocean Thermal Energy Conversion (OTEC), Minami Beach, pp. 237–260.
Tan, Y., Wang, G., Wang, S., Cui, N., 1990. An experimental research of spray falling film boiling on the second generation mechanically made porous surface tubes, Proceedings of the 9th International Heat Transfer Conference. Hemisphere Pub, Jerusalem, Israel, pp. 269–273.
Thome, J.R., 1999. Falling film evaporation: state-of-the-art review of recent work. J. Enhanc. Heat Transfer 6, 263–277.
Webb, R.L., Pais, C., 1992. Nucleate pool boiling data for five refrigerants on plain, integral-fin and enhanced tube geometries. Int. J. Heat Mass Transf. 35, 1893–1904.
Yang, S.M., Tao, W.Q., 2006. Heat Transfer, fourth ed. Higher Education Press, Beijing, China.
Zeng, X., Chyu, M.C., 1995. Heat transfer and fluid study of ammonia spray evaporators, ASHRAE Research Report. Texas Tech University, Lubbock, Texas.
Zeng, X., Chyu, M.C., Ayub, D.Z.H., 2000. Ammonia spray evaporation heat transfer performance of single low-fin and corrugated tubes, Proceedings of The ASME-ZSITS International Thermal Science Seminar Bled Slovenia, pp. 325–332.
Zeng, X., Chyu, M.C., Ayub, Z.H., 2001. Experimental investigation on ammonia spray evaporator with triangular-pitch plain-tube bundle, part II: evaporator performance. Int. J. Heat Mass Transf. 44, 2081–2092.
Zhao, C.Y., Jin, P.H., Ji, W.T., Tao, W.Q., 2016a. Heat transfer correlation of the falling film evaporation on a single horizontal smooth tube. Appl. Therm. Eng. 103, 177–186.
Zhao, C.Y., Jin, P.H., Ji, W.T., Tao, W.Q., 2016b. Cross vapor stream effect on falling film evaporation in horizontal tube bundle using R134a. Heat Transfer Eng. Accepted.